

LOAD CARRYING CAPACITY AND DUCTILITY OF RC COLUMNS CONFINED BY CARBON FIBER REINFORCED POLYMERS

*Sung-Chul Chun, DICT, Daewoo E&C Co., Ltd., Suwon, Korea
Hyung-Chul Park, DICT, Daewoo E&C Co., Ltd., Suwon, Korea*

Abstract

External confinement of concrete can significantly enhance its strength and ductility, resulting in large energy dissipation capacity. Therefore, confined RC columns have larger bending moment capacity and ductility, as well as larger axial load carrying capacity. A new strengthening technique using Fiber Reinforced Polymers (FRP) was introduced instead of the conventional methods such as steel plate jackets and reinforced concrete jackets.

The objectives of this research are to investigate the behavior of eccentrically loaded RC columns confined by Carbon Fiber Reinforced Polymers (CFRP) jackets and to analyze the enhanced load carrying capacity and ductility. To evaluate the performance, especially for the axial force-bending moment interaction relationship of the RC columns confined by CFRP, a series of eccentric loading tests (4 unconfined columns and 5 confined columns) have been conducted. Furthermore analytical studies using stress-strain models of confined concrete have been performed. The stress-strain model of confined concrete, based on the passive confinement mechanism by Madas, P. and Elnashai, A. S. (1992), was used as the compressive zone in the analysis. For comparison, Mander, J. B. et al.'s stress-strain model (1988) was also used. The analytical results compared with the experimental results show that the analysis using the proposed model can evaluate load carrying capacity properly. Since the CFRP's linearly elastic characteristic is considered in the proposed model, the suggested analytical method can theoretically support the enhancement of ductility of confined RC columns.

Keywords: Carbon Fiber Reinforced Polymers (CFRP); confinement; P-M interaction diagram; load carrying capacity; ductility; repair

Introduction

Reinforced Concrete (RC) columns deteriorate with age and are damaged by the overloads, mainly from earthquake. It is necessary to strengthen the deteriorated and damaged RC columns to increase the carrying capacity against axial load and bending moment, and the ductility for the improved seismic performance. Steel plate jackets and reinforced concrete jackets have been widely used to strengthen the RC columns. However, they have several problems because of their material characteristics.

Since steel is isotropic material, it is difficult to uncouple or optimize its resistance to the axial and the circumferential loads. Also, its high modulus of elasticity exerts a large portion of axial load to the steel jacket, resulting in premature buckling. Furthermore, the Poisson's ratio of steel is higher than that of concrete at the early stage of loading. This differential expansion results in partial separation of two materials, delaying the activation of confinement mechanism. Besides, outdoor use of steel jackets in corrosive environment can be expensive.

Reinforced concrete jackets are comparatively cheap and do not require special design and construction techniques. However, their longer construction period due to curing requirement and the enlargement of column size are major disadvantages.

To solve the above problems, Fiber Reinforced Polymers (FRP) was recently introduced as an

alternative and many research efforts have been made to provide the additional confinement to the concrete using FRP.^{1,2,3} The major benefit of FRP is its orthotropic behavior that prevents the interaction between the jacket and concrete in axial direction, resulting in the early activation of its confinement. Other benefits of FRP are high strength, light weight, resistance to corrosion, low cost, versatility, etc.¹

The researches on the confinement mechanism of steel spirals/hoops have been conducted and the analytical models have been proposed.^{4,5,6,7} However, an analytical model for the confinement behavior of FRP considering its linear elasticity has not been established yet. Also, the implementation of CFS requires understanding of the confined columns' behavior and an analytical model for estimating its strength and ductility.

The authors previously proposed the analytical model called Passive Confinement Model (PCM) for the confined concrete with Carbon Fiber Sheets (CFS)¹¹. This paper verifies PCM by conducting a series of eccentric loading tests.

Analytical Models for Confinement Mechanism

Load carrying capacity and ductility of the confined columns can be estimated by rationally modeling the stress-strain relationship. This study verifies PCM and compares PCM with Mander et al.'s model.

Passive Confinement Model (PCM)

CFS provides additional confinement to the RC columns as the CFS elongates. The confining force is proportional to the amount of CFS's elongation, and this force changes the Poisson's ratio and strength of the concrete. As the Poisson's ratio changes, the expansion rate also changes, and new confinement is imposed to the concrete. Kestner, J. et al. (1997)⁸ developed the Variably Confined Concrete Model (VCCM) based on Madas, P. and Elnashai, A. S.' model (1992, see Figure 1)⁹ considering this passive confinement mechanism.

The authors previously proposed the Passive Confinement Model (PCM) based on VCCM, and performed the concentric loading tests to develop the model.^{10,11} In PCM, the Poisson's ratio-confinement relationship and the determinant factors for the maximum confining pressure were reflected. The following explains the step-by-step procedure:

Step 1. An axial strain ε_c is chosen.

Step 2. The Poisson's ratio ν is determined.

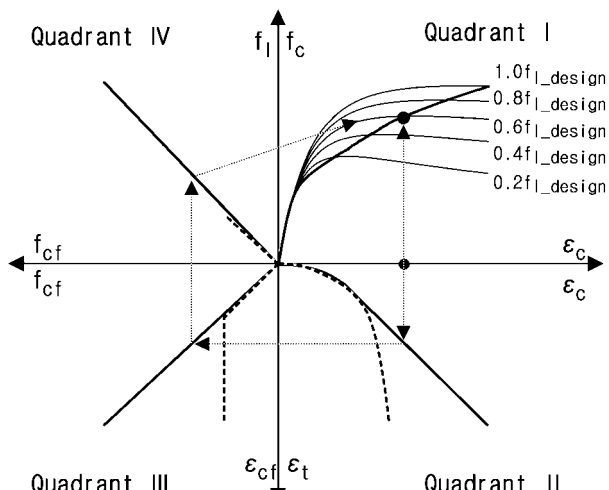
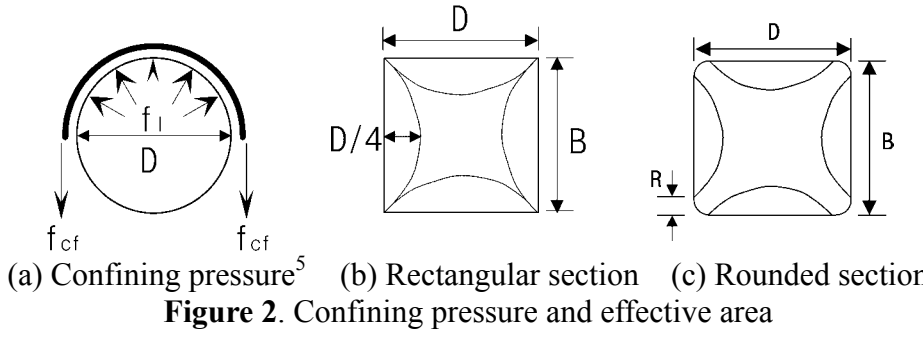


Figure 1. Stress-strain relationship model for concrete having variable confinement⁹



With adequate amount of external fiber composites, lateral expansion of concrete can be effectively restrained. Therefore, the Poisson's ratio of the confined concrete converges to a constant value with increasing axial strain. The convergent value is defined as the ultimate Poisson's ratio ν_u . This phenomenon is an unique characteristic of CFS-confined concrete. The ultimate Poisson's ratio ν_u is determined by eq. (1) according to design confinement ratio f_{ld}/f_{co} defined by eq. (3), which was obtained from the concentric loading test of CFS-confined concrete conducted by the authors.¹¹ The Poisson's ratio during elastic state before reaching the ultimate Poisson's ratio follows eq. (2).^{9,12}

$$\nu_u = -0.2305 \ln(f_{ld} / f_{co}) + 0.087 \quad (1)$$

$$\nu = \nu_o [1.0 + 1.3763x - 5.36x^2 + 8.586x^3] \leq \nu_u \quad (2)$$

Where f_{ld} is designed confining pressure; f_{co} is peak compressive strength of unconfined concrete; $x = \varepsilon_c / \varepsilon_{cc}$; ν_o is a initial Poisson's ratio of concrete; and ε_{cc} is an axial strain corresponding to peak axial stress, f_{cc} , of confined concrete. Design confining pressure f_{ld} is calculated from eq. (3).

$$f_{ld} = (2f_{cf}t_{cf}/D)\kappa_s + (A_c/A_g)f_{lhu} \quad (3)$$

Where κ_s is shape factor; f_{cf} is tensile strength of CFS; t_{cf} is thickness of CFS; D is width of section; A_c is area of concrete surrounded by hoops/spirals; A_g is gross concrete area; and f_{lhu} is the maximum confining pressure provided by hoops/spirals, given by Mander et al..⁵

Confining pressure f_l can be determined from the equilibrium of force in the free-body diagram for any sector of the confined section (see Figure 2(a)). Design confining pressure f_{ld} is determined when the strain of CFS reaches the maximum strain. When hoops or spirals are used, the confining pressure by hoops or spirals should be added to the confining pressure by CFS, considering confining area ratio (A_c/A_g). The shape factor κ_s , given by Mander et al., can be determined by the ratio of effectively confined concrete area to the gross area of the section (see Figure 2(b)). κ_s for circular columns is 1.0, and that for rectangular columns is 0.33. In practice, the corners of the rectangular column are rounded to prevent the premature failure of CFS. In this case, the shape factor can be defined as eq. (4).²

$$\kappa_s = \frac{1 - \left(\frac{(B-2R)^2 + (D-2R)^2}{3DB} \right) - \rho}{1 - \rho} \quad (4)$$

Where R is radius of corner; and ρ is longitudinal reinforcement ratio of section.

Step 3. The transverse strain ε_t , corresponding to the axial strain, is determined by eq. (5). Complete composite action between confining composite materials and concrete columns is assumed.

$$\varepsilon_t = \varepsilon_{cf} = \nu \varepsilon_c \quad (5)$$

Where ε_{cf} is the strain of CFS

Step 4. The confining pressure f_l is determined. It is assumed that the core concrete is confined

by both hoops/spirals and CFS. However, the cover concrete is confined by CFS only. The additional confinement by hoops/spirals on core is proportional to the lateral strain until the transverse steel yields, but it is constant after yielding, which is shown in eq. (7).

$$\begin{aligned} f_l &= \left(2 \varepsilon_{cf} E_{cf} t_{cf} / D\right) \kappa_s && (\text{cover concrete}) \\ &= \left(2 \varepsilon_{cf} E_{cf} t_{cf} / D\right) \kappa_s + f_{lh} && (\text{core concrete}) \end{aligned} \quad (6)$$

$$\begin{aligned} f_{lh} &= f_{lhu} \frac{\varepsilon_t}{f_{yh}/E_s} && (\varepsilon_t \leq f_{yh}/E_s) \\ &= f_{lhu} && (\varepsilon_t > f_{yh}/E_s) \end{aligned} \quad (7)$$

Where E_{cf} is elasticity modulus of CFS; f_{lh} is confining pressure provided by spirals/hoops; E_s is elasticity modulus of steel; and f_{yh} is yield strength of hoops/spirals.

Step 5. With the confining pressure f_l , the peak compressive strength of confined concrete f_{cc} and corresponding strain ε_{cc} are determined by eqs. (8), (9).⁵

$$f_{cc} = f_{co} \left(2.254 \sqrt{1 + 7.94 f_l / f_{co}} - 2 f_l / f_{co} - 1.254 \right) \quad (8)$$

$$\varepsilon_{cc} = \varepsilon_{co} \left(5 f_{cc} / f_{co} - 4 \right) \quad (9)$$

Where ε_{co} is axial strain corresponding to peak axial stress f_{co} of unconfined concrete (generally 0.002).

The axial strain ε_{cc} , calculated from eq. (9), should be compared with the assumed value at Step 2. If the difference between the two values exceeds the tolerance, return to Step 2 with refined ε_{cc} . In this study, the tolerance was 1%.

Step 6. The axial stress f_c , corresponding to the chosen axial strain ε_c , is calculated by eq. (10).¹³

$$f_c = f_{cc} \frac{\varepsilon_c}{\varepsilon_{cc}} \left(\frac{n}{n-1 + (\varepsilon_c / \varepsilon_{cc})^n} \right) \quad (10)$$

Where $n = E_c / (E_c - f_{cc} / \varepsilon_{cc})$, and E_c is modulus of elasticity for concrete.

Mander, J. B. et al.'s model

Mander et. al.⁵ proposed the relationships (eq. (8)~(11)) for the confined concrete (see Figure 3). The ultimate concrete compressive strain ε_{cu} is determined from eq. (11), when the strain of CFS ε_{cf} reaches ultimate strain of CFS ε_{cfu} .

$$U_{cf} + U_{sh} = U_{cv} + U_{cr} + U_{sl} - U_{co} \quad (11)$$

Where U_{cf} is ultimate strain energy capacity of the CFS; U_{sh} is absorbed strain energy by hoops/spirals until CFS fractures; U_{cv} is ultimate strain energy of the cover concrete confined by CFS; U_{cr} is ultimate strain energy of the core concrete confined by CFS and hoops/spirals; U_{sl} is energy required to maintain yield in longitudinal steel in compression; and U_{co} is ultimate strain energy of the unconfined concrete.

Longitudinal Steel

In confined RC columns, the strain hardening effect of the longitudinal steel should be considered as the compressive strain of confined concrete greatly increases. Three equations are required for this model,^{6,14} and each value comes from the coupon test (see Table 2).

$$f_s = f_y \left[\frac{m(\varepsilon_s - \varepsilon_{sh}) + 2}{60(\varepsilon_s - \varepsilon_{sh}) + 2} + \frac{(\varepsilon_s - \varepsilon_{sh})(60 - m)}{2(30r + 1)^2} \right] \quad (12)$$

Where $\varepsilon_{sh} \leq \varepsilon_s \leq \varepsilon_{su}$; ε_y is yield strain; ε_{sh} is steel strain at commencement of strain hardening; ε_{su} is tensile fracture strain of steel; $r = \varepsilon_{su} - \varepsilon_{sh}$; $m = ((f_{su}/f_y)(30r+1)^2 - 60r - 1)/(15r^2)$; $f_y = 392 \text{ MPa}$; and $f_{su} = 662 \text{ MPa}$.

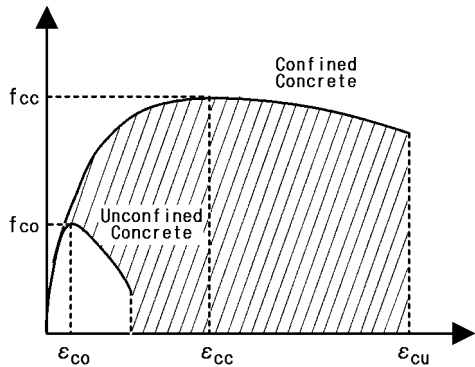


Figure 3. Stress-strain model of confined concrete⁵

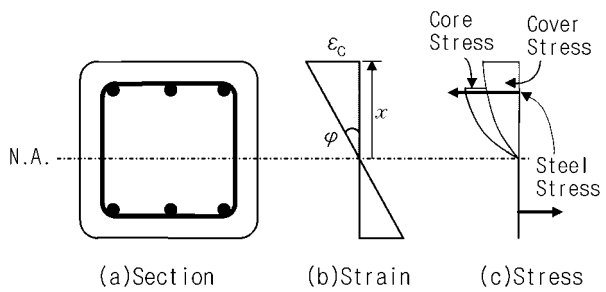


Figure 4. Assumed strain and stress distribution

Analysis Method

The load carrying capacities of the confined columns are obtained by using previous models with varying the location of the neutral axis. It is assumed that a strain distribution is linear and the deformed section remains plane. Because of the different confinement, the core and cover concrete at the same distance from the neutral axis have the same strain, but different stresses (see Figure 4).

The axial load and moment carrying capacities are determined from the force equilibrium, and the curvature is the compressive strain divided by the depth of the neutral axis.

Experiment

The verification of PCM was performed with P-M interaction diagramming, and the eccentric loading test results were compared with analytical results. The axial loading capacity (P_o) was obtained from the concentric loading test, and the eccentric loading tests were performed under constant axial load of $0.0P_o$, $0.25P_o$, $0.5P_o$, $0.75P_o$. The test matrix is described in Table 1.

Specimen Layout

Each specimen consisted of a single column with a stub as shown in Figure 5. The 200mm square by 1,000mm tall column contained six deformed bars of 13mm diameter. D10 hoops spaced at 100mm were used as transverse reinforcement, and the region of lateral load applied was strengthened with hoops spaced at 50mm. The section size was selected based on the capacity of 2,000kN actuator for concentrically loaded retrofitted column test. As shown in Figure 5, the corners were rounded to an approximately 30mm radius to prevent stress concentration that may cause premature failure of CFS at the corners. Retrofitted specimens were wrapped with 2-ply unidirectional CFS jacket.

Material Properties

The ready-mixed concrete with design compressive strength (f'_c) of 21MPa was used. The 28-day compressive strength of the concrete and the measured properties of reinforcement steels are presented in Table 1 and Table 2, respectively. The resin and CFS were produced by a Japanese company with the properties in Table 3.

Test Setup and Instrumentation

Figure 6 shows the test setup. The stub was fastened to the strong floor with six high-strength rods, and each rod was prestressed to 200kN to prevent slip and overturning under large lateral load.

An axial load was applied to the test column using two center-hole-oil jacks and high strength rod before applying lateral load. The force was transferred to the column by a cross beam mounted on the top of specimen. The device for keeping constant pressure was attached to the jack to prevent

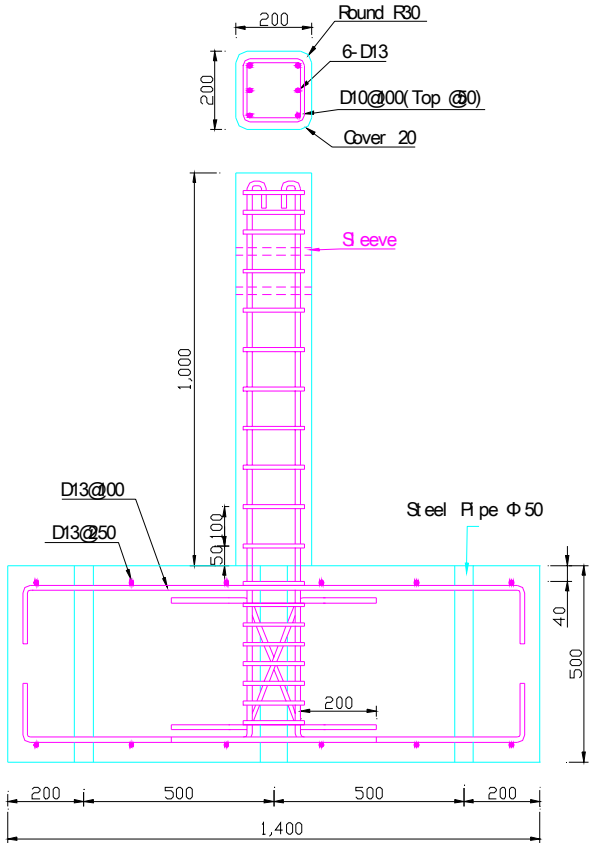


Figure 5. Detail of test column (dimensions in mm)

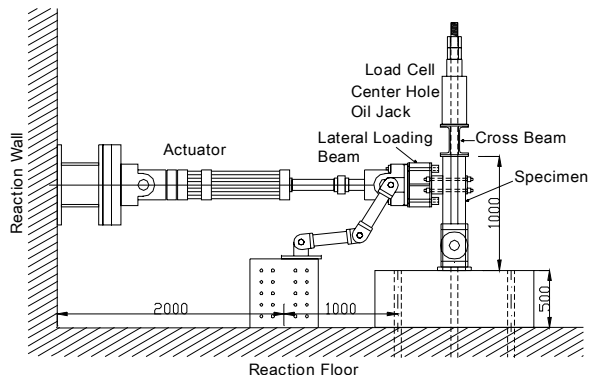


Figure 6. Test setup (dimensions in mm)

pressure variation of the oil jack due to force relaxation of high strength rod and lateral displacement of the specimen. The lateral load using 500kN capacity actuator was monotonically imposed at 750mm level from the column bottom. The twist of column was prohibited by the device that is attached to the lateral loading beam.

To measure the lateral displacement, three displacement transducers at 750mm level from the column bottom and two transducers at 1,000mm level were used. To determine the curvature within the plastic hinge region, two displacement transducers were installed vertically at the both sides of the column. Six strain gauges at longitudinal steels and eight at the lowest hoop were placed respectively.

Test Results

(1) Observed Behavior

Table 1. Test matrix

Specimen	Axial load		f'_c [MPa]	Remark
	P, [kN]	P/Po		
EN-P00	0	0%	21.0	Control
EN-P25	246	27%		
EN-P50	456	50%		
EN-Po	912	100%		
ER-P00	0	0%	26.1	Retrofit (2 Plies)
ER-P25	360	23%		
ER-P50	707	45%		
ER-P75	1,026	66%		
ER-Po	1,562	100%		

E①-P②: ① R=Retrofit, N=Control; ② P/Po Ratios

Table 2. Properties of rebar

Rebar	Yield strength [MPa]	Tensile strength [MPa]	Elastic modulus [GPa]	Elongation [%]
D10	387.8	596.8	182	24.7
D13	386.3	662.3	188	22.1

Table 3. Properties of CFS and epoxy resin

Carbon fiber sheet	Tensile strength [MPa]	Elastic modulus [GPa]	Thickness [mm]
	3,479	230	0.11
Epoxy resin	Tensile strength [MPa]	Compressive strength [Mpa]	Flexural strength [MPa]
	49.7	79.7	67.8

Table 4. Test results

Specimen	P [kN]	Max. moment state			Major Failure Mode	Specimen	P [kN]	Max. moment state			Major Failure Mode
		M [kN& m]	δ [mm]	ϕ [m ⁻¹]				M [kN& m]	δ [mm]	ϕ [m ⁻¹]	
EN-P00	0	32	135.1	-	Reduction of moment capacity after large deformation	ER-P00	0	35	118.4	-	Tensile rebar fracture
EN-P25	246	38	25.9	0.161	Buckling of compressive longitudinal steel	ER-P25	360	56	58.2	0.379	CFS fracture(center)
EN-P50	456	39	15.9	0.093	after spalling and crushing of concrete in compression zone	ER-P50	707	64	57.4	0.381	CFS fracture(edge)
EN-Po	912	0	0.0	-		ER-P75	1,026	61	44.6	0.278	CFS fracture(edge)
						ER-Po	1,562	0	0.0	-	CFS fracture(edge) & debonding of CFS

Note: P = Axial load; M = Moment; δ = Lateral displacement; ϕ = Curvature; 1kN = 225lb; 1mm = 0.0394in

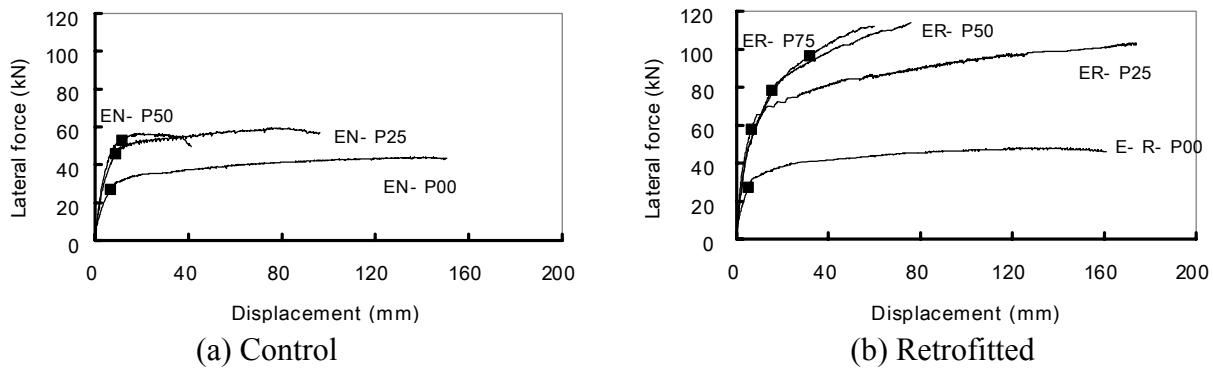


Figure 7. Load versus lateral displacement

It was observed at the control specimens that the load carrying capacity reduced with spalling of the cover concrete in compression zone after reaching the maximum load. However, the load carrying capacity of the retrofitted specimens increased slowly and steadily after yielding of tensile reinforcement steels, and the ductile failure mode was observed even for the specimens under higher constant axial load (see Figure 7). ER-P00 failed with fracture of tensile reinforcement, but other retrofitted specimens failed with fracture of CFS in compression region. From all the retrofitted specimens, bulging of the jacket in the transverse direction and wrinkle near the bottom of the jacket were observed. Before CFS jacket completely fractured, partial fractures were observed at the wrinkled area without any reduction of the load carrying capacity.

Figure 8 shows the final appearance of the specimens. Test results are summarized in Table 4. Lateral force-displacement curves of control and retrofitted specimens are provided in Figure 7.

(2) P-M Interaction Diagram

Figure 9 is the P-M interaction diagram of both the control and the retrofitted columns. The confined columns have larger bending moment capacity, ductility and axial load carrying capacity than the control columns. If the difference of concrete strengths between the control and the retrofitted column is ignored, axial load and bending moment carrying capacity increase about 70% and 10%, respectively.

The relation between the increment of load carrying capacity and the eccentricity (e/h) is shown in Figure 10. K_s is defined by eq. (13) as the ratio of the length from the origin to the P-M curve of the

retrofitted column under a certain eccentricity to that of the control column.

$$K_s = \frac{\sqrt{P_r^2 + M_r^2}}{\sqrt{P_n^2 + M_n^2}} = \frac{P_r}{P_n} = \frac{M_r}{M_n} \quad (13)$$

Where subscripts, r and n , stand for the retrofitted and the control, respectively.

As shown in Figure 9 and Figure 10, the pure bending moment capacity increases slightly. However when $e/h=1.0$, K_s is about 1.5. The increment of the ultimate moment is less than that of the ultimate axial load. This is not a shortcoming of this strengthening method, since the columns that



Figure 8. Failure for selected specimens

require retrofitting lack adequate ductility, not flexural capacity.

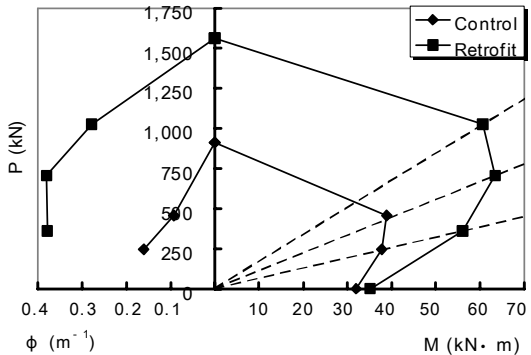


Figure 9. P-M interaction diagram and curvature

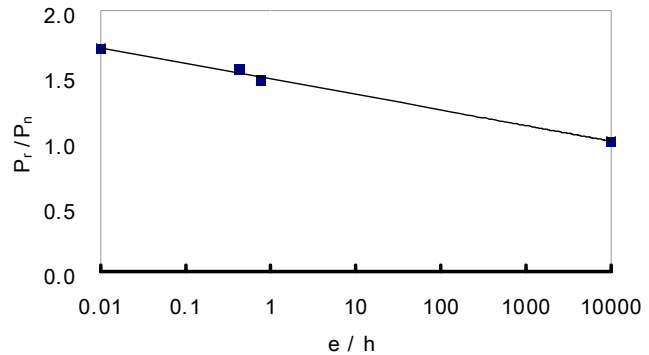


Figure 10. Strength increment versus eccentricity

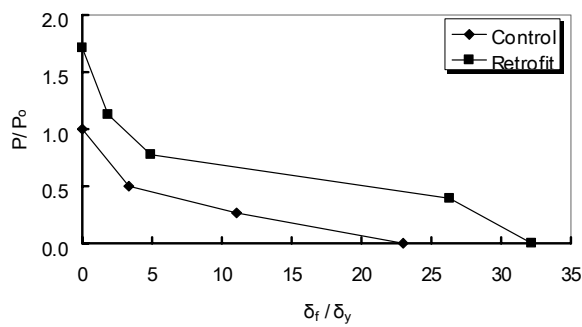


Figure 11. Ductility factor

The axial load carrying capacity improves as the compressive strength of confined concrete enhances. Also, the ductility of concrete improves, and the tensile reinforcing steels undergo strain hardening range, resulting in the increment of bending moment carrying capacity.

The curvature at the maximum moment of each specimen is shown in left side of Figure 9. The curvatures of the retrofitted columns improve greatly than those of the control columns. The curvatures of specimens without axial load (EN-P00, ER-P00) could not be measured because of extremely large deformation.

(3) Ductility

Ductility is a desirable feature of any structural design as it safeguards a structure against unpredicted overloading and/or load reversal. Ductility factor is given as the ratio of displacement at failure (δ_f) to that at yielding (δ_y). δ_f is the displacement when the specimen fails apparently, e.g. fracture of tensile steel or CFS in retrofitted specimens, or when the strength reduces to 85% of the ultimate strength¹⁵ (However in EN-P00 and EN-P25, tests were terminated before the strength reduced to 85% of the ultimate strength because of severe deformation).

According to Samra (1990)¹⁶, a displacement ductility factor of more than 4.0 is required for seismic design. The test results show that the ductility factor of the control specimens for which the axial load is within 40% of the axial load carrying capacity P_o is more than 4.0. Figure 11 shows the displacement ductility factor with varying axial load. The retrofitted specimens have ductility factor of more than 4.0 until the axial load is within 90% of axial load carrying capacity of the control column (EN-Po), or 53% of that of the retrofitted column (ER-Po). Compared with the column made of normal strength concrete, the axial strength of column made of high strength concrete increases but the ductility decreases.^{15,17} However, when the column is retrofitted with CFS, sufficient ductility can be obtained.

Comparisons

P-M Interaction Diagram When Premature Failure of CFS Is Not Considered

Because the appearances of fracture of CFS were mixed with tensile failure at center/edge and debonding of sheet, it is assumed that the maximum strain of CFS at fracture is the ultimate strain, $\varepsilon_{cfu} = 0.015$. Figure 12 shows the experimental and analytic P-M interaction and curvature diagrams.

The capacities of analytical results are lower than those of the test results except for the concentrically loaded specimens (EN-Po, ER-Po). In control specimens, it seems that the axial strain of concrete is higher than 0.003 assumed in analysis because of the hoop confinement. Therefore, the bending moment capacity and the curvature from the test results are higher than those from the analysis.

In retrofitted specimens, analytically obtained capacities from PCM are lower than those from the test results in axial load range of 30~70% of axial load of ER-Po, and higher in the other range. As the premature failure at edge of CFS occurred at ER-Po, the axial capacity from the test is lower than that from the analytical result. According to the previous studies on the concentric loading test of concrete confined by CFS,^{2,11} the effective maximum strain of CFS should be restricted to account for the premature failure from the debonding of sheets and stress concentration at the column corners.

As described previously, bulging of the CFS in transverse direction happened for all retrofitted specimens before failure. This phenomenon increases the effective depth of the compression zone, and may increase the bending moment carrying capacity.

The measurement error, the possibility of local failure, difference of plastic hinge location, etc. make it difficult to predict the exact curvature. However, analysis using PCM can properly explain the increment of ductility.

Analysis using Mander et al.'s model shows the lower bending moment carrying capacities at lower axial load ratio (P/P_o) region. Besides, it can be seen that curvatures of analysis are far lower than those of the test results and analysis using PCM. Mander et al.'s model was originally developed for the confinement of reinforcement hoops/spirals. Yield strain of steel is far lower than the ultimate strain of steel, therefore the confining pressure in Mander et al.'s model is fixed at maximum value. But CFS has the linear stress-strain relationship until fracture, thus the real confining pressure varies with expansion of concrete. In Mander et al.'s model, compressive strength is reached quickly, i.e. axial strain corresponding to compressive strength is lower than that of the experimental result. Moreover, because ε_{cc} corresponding to compressive strength is obtained by simplified relationship as eq. (8) not considering geometric (strain) compatibility between the core and the CFS, ε_{cc} is lower than the real value. Consequently, lower curvature and bending moment carrying capacity are estimated.

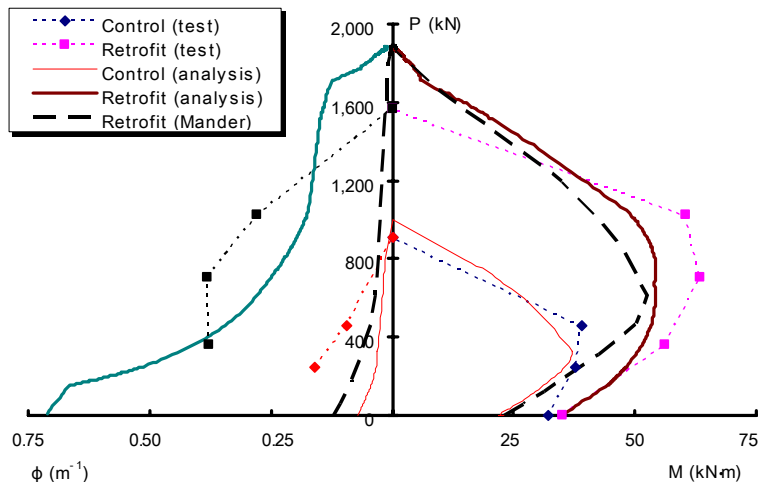


Figure 12. P-M interaction diagram and curvature (comparison test with analysis)

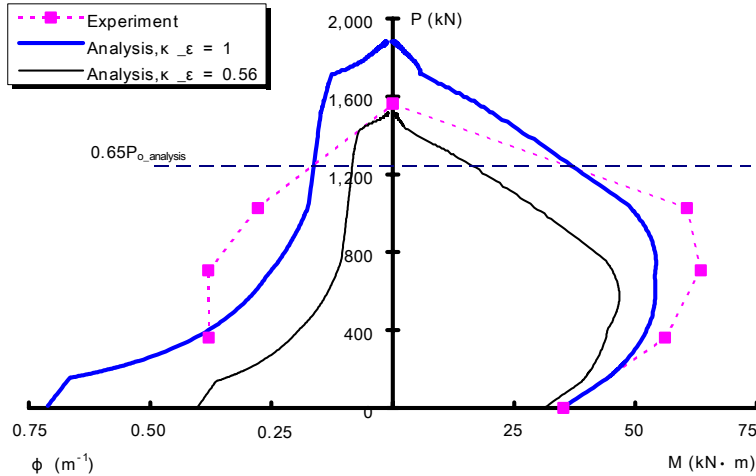


Figure 13. P-M interaction diagram and curvature (varying $\kappa_e=1.0, 0.56$)

P-M Interaction Diagram When Premature Failure of CFS Is Considered

The authors' previous study¹¹ on the concentric loading test of square concrete column confined by CFS suggested that the effective maximum strain of CFS should be reduced to 56% of the ultimate strain (0.015) considering the premature failure. Results from the reduced maximum strain of CFS and PCM analysis are shown in Figure 13.

Because the effective maximum strain of CFS reduces, the compressive strength and the corresponding strain decrease. In consequence, both the axial load carrying capacity and the curvature decrease. As the bending moment carrying capacity is not sensitive to the compressive strength of concrete, the moment carrying capacity decreases little. However, the curvature of the specimen without axial load greatly decreases because of the reduction of the ultimate concrete strain and the enlargement of the compressive zone depth.

Compared with the test result, the axial load carrying capacity of ER-Po considering the premature failure of CFS is properly predicted. However, for the specimens with lower axial load (P/P_o), differences of bending moment carrying capacity and curvature considering premature failure between the test and the analysis are large. According to the observed behavior of tests, the tensile fracture of CFS in all retrofitted specimens except ER-Po occurred. Therefore, the maximum CFS strains of those specimens were larger than that of the concentrically loaded specimen. As shown in Figure 13, when premature failure is not considered, the analytical bending moment carrying capacity and the curvature can be conservative under the applied axial load lower than 65% of analytical axial load carrying capacity.

As the axial load ratio (P/P_o) increases, possibility of premature failure increases. In analysis of confined column, it can be suggested that the effective strain of CFS be reduced proportionally to the axial load ratio P/P_o .

Conclusion

To evaluate the performance of RC columns confined by Carbon Fiber Sheets (CFS), a series of eccentric loading tests were conducted. Furthermore, analytical studies using a PCM considering CFS' linearly elastic characteristics were performed. P-M interaction diagrams and curvatures at the maximum moment of retrofitted columns were obtained analytically, and were compared with the test results. Based on this study, the following conclusions were made:

- (1) The axial load carrying capacity of the confined columns improves, because the compressive

- strength of the confined concrete enhances by the confinement effect.
- (2) The ultimate strain of the confined concrete increases. Consequently, the tensile reinforcement steels undergo strain hardening range resulting in increment of the bending moment carrying capacity and the ductility. Increment of the ductility provides higher reliability of the confined columns.
- (3) The comparison of the analytical and the experimental results shows that the analysis using PCM can properly predict the P-M interaction diagram and the curvature. However, for more accurate estimation of the bending moment capacity, the effective maximum strain of CFS should be reduced as the axial load increases to account for the premature failure of CFS.
- (4) Compared with the experimental results, the maximum curvature from PCM is underestimated in overall. Although PCM can not predict the exact moment-curvature relationship, this theoretically explains the enhancement of the ductility of the confined column.

References

1. Saadatmanesh, H.; Ehsani, M. R.; and Li, M. W., "Strength and Ductility of Concrete Columns Externally Reinforced with Fiber Composite Straps," *ACI Structural Journal*, July-Aug. 1994, pp. 434-447
2. Harries, K. A.; Kestner, J.; Pessiki, S.; and Ricles, J., "Axial Behavior of Reinforced Concrete Columns Retrofit with FRPC Jackets." *Proceedings, 2nd International Conference on Composites in Infrastructure*, University of Arizona, 1997, pp. 411-425
3. Mirmiran, A. and Shahawy, M., "Behavior of Concrete Columns Confined by Fiber Composites" *Journal of Structural Engineering*, ASCE, May 1997, pp. 583-590
4. Ahmad, S. H., and Shah, S. P., "Complete triaxial stress-strain curves for concrete." *Journal of Structural Engineering*, ASCE, V. 108, No. ST4, Apr. 1982, pp. 728-742
5. Mander, J. B.; Priestley, M. J. N.; and Park, R., "Theoretical Stress-Strain Model for Confined Concrete." *Journal of Structural Engineering*, ASCE, V. 114, No. 8, Aug. 1988, pp. 1804-1826
6. Park, R., and Paulay, T., *Reinforced Concrete Structures*, John Wiley and Sons, New York, N.Y., 1975, pp. 21-30
7. Saatcioglu, M., and Razvi, S. R., "Strength and ductility of confined concrete." *Journal of Structural Engineering*, ASCE, June 1992, 118(6), 1590-1607
8. Kestner, J.; Harries, K. A.; Pessiki, S. P.; Sause, R.; and Ricles, J. M., "Rehabilitation of Reinforced Concrete Columns Using Fiber Reinforced Polymer Composite Jackets," *Lehigh University ATLSS Report* No. 97-07, July 1997, pp. 12-13
9. Madas, P. and Elnashai, A. S., "A New Passive Confinement Model for the Analysis of Concrete Structures Subjected to Cyclic and Transient Dynamic Loading," *Earthquake Engineering and Structural Dynamics*, Vol. 21, 1992, pp.409-431
10. Chun, S. C.; Park, H. C.; Ahn, J. H.; and Park, C. L., "Experimental Study on Strength of Concrete Confined by Carbon Fiber Sheets," *AIK Proceedings*, Vol. 18, No. 2, Oct. 1998, pp. 335-340 (in Korean)
11. Chun, S. C.; Kim, J. Y.; Park, H. C.; Park, C. L., "A Stress-Strain Model of Concrete Confined by Carbon Fiber Sheets," *Journal of the Architectural Institute of Korea, Structure & Construction Section*, Vol. 15, No.1, Jan. 1999, pp. 27-36 (in Korean)
12. Elwi, A. A., and Murray, D. W., "A 3D Hypoelastic Concrete Constitutive Relationship," *Journal of the Engineering Mechanics Division*, ASCE, Vol. 105, No. 4, Apr. 1979, pp. 623-641
13. Popovics, S., "A Numerical Approach to the Complete Stress-Strain Curves for Concrete," *Cement and Concrete Research*, Vol. 3, No. 5, 1973, pp. 583-599
14. Samra, R. M.; Deeb, Nidal A. A.; and Madi, Usama R., "Transverse Steel Content in Spiral Concrete Columns Subject to Eccentric Loading", *ACI Structural Journal*, Vol. 93, No. 4, July-Aug. 1996, pp. 412-419
15. Foster, Stephen J., and Attard, Mario M., "Experimental Tests on Eccentrically Loaded High Strength Concrete Columns," *ACI Structural Journal*, Vol. 94, No. 3, May-June 1997, pp. 295-303
16. Samra, R. M., "Ductility Analysis of Confined Columns," *Journal of Structural Engineering*, ASCE, Vol. 116, No. 11, Nov. 1990, pp. 3148-3161
17. Diniz, Sofia M. C., and Frangopol, Dan M., "Strength and Ductility Simulation of High-Strength Concrete Columns," *Journal of Structural Engineering*, ASCE, Vol. 123, No. 10, Oct. 1997, pp. 1365-1374